

# UC Berkeley

## UC Berkeley Previously Published Works

### Title

On the Role of Switch Output Capacitance on Passive Balancing Within the Flying Capacitor Multilevel Converter

### Permalink

<https://escholarship.org/uc/item/1q1720kp>

### Journal

IEEE Transactions on Power Electronics, 40(2)

### ISSN

0885-8993 1941-0107

### Authors

Bayliss, Roderick S, III

Brooks, Nathan C

Pilawa-Podgurski, Robert C. Nn

### Publication Date

2025-02-01

### DOI

10.1109/TPEL.2024.3493832

Peer reviewed

©2025 IEEE

*IEEE Transactions on Power Electronics*, vol. 40, no. 2, pp. 3275-3285, Feb. 2025

## **On the Role of Switch Output Capacitance on Passive Balancing within the Flying Capacitor Multilevel Converter**

Roderick S. Bayliss III  
Nathan C. Brooks  
R. C. N. Pilawa-Podgurski

Personal use of this material is permitted. Permission from IEEE must be obtained for all other uses, in any current or future media, including reprinting/republishing this material for advertising or promotional purposes, creating new collective works, for resale or redistribution to servers or lists, or reuse of any copyrighted component of this work in other works.

# On the Role of Switch Output Capacitance on Passive Balancing within the Flying Capacitor Multilevel Converter

Roderick S. Bayliss III, *Student Member, IEEE*, Nathan C. Brooks, *Student Member, IEEE*, Robert C. N. Pilawa-Podgurski, *Fellow, IEEE*

**Abstract**—Flying capacitor multilevel (FCML) converters typically rely on natural balancing to achieve a balanced distribution of flying capacitor voltages. The mechanisms by which the flying capacitor voltages are able to balance have been extensively studied and theoretically there are certain combinations of level count and duty cycle at which the flying capacitor voltages do not balance. Although the flying capacitor voltages should diverge from the balanced distribution, in practice this behavior is rarely observed. To resolve this discrepancy between FCML converter theory and experiment, this article analyzes the impact of switch output capacitance on the flying capacitor voltage balancing dynamics, and illustrates that this capacitance has a naturally balancing effect. The additional mechanism of switch output capacitance induced balancing is analytically described and compared against experimental results on several FCML converter prototypes.

## I. INTRODUCTION

**P**OWER converters in applications such as traction and propulsion drives and data center power delivery require high power density and efficiency [1]–[3]. In pursuit of maximizing these objectives, the flying capacitor multilevel (FCML) converter has emerged as a promising topology for these cutting edge applications [4]–[8]. Although the topology was initially developed to remedy the lack of high voltage switches rated for the input voltage in high voltage power conversion applications [9], the FCML converter is able to outperform conventional topologies in lower voltage applications. A simplified schematic of a five-level FCML converter is presented in Fig. 1. A key practical challenge in the utilization of high-performance FCML converters is the voltage balancing of the flying capacitors, the focus of this work. Specifically, we demonstrate the effect of transistor output capacitance

Part of this manuscript was presented at the 2022 IEEE Workshop on Control and Modeling for Power Electronics (COMPEL) as the paper “On the Role of Switch Output Capacitance on Passive Balancing within the Flying Capacitor Multilevel Converter”. This manuscript extends the previous work by including the impact of source impedance on flying capacitor voltage balancing and comparing this impact to that of  $C_{oss}$ -induced charge flow. Additionally, we extend our previous model to include the nonlinear capacitances which are typically found in high performance power converters. Roderick S. Bayliss III and Robert C. N. Pilawa-Podgurski are with the Department of Electrical Engineering and Computer Sciences, University of California, Berkeley, CA U.S.A. (e-mail: rodbay@berkeley.edu; pilawa@berkeley.edu).

Nathan C. Brooks is with the Department of Electrical and Computer Engineering, Rose-Hulman Institute of Technology, Terre Haute, IN, U.S.A. During the duration of this work, Nathan C. Brooks was with the Department of Electrical Engineering and Computer Sciences, University of California, Berkeley.

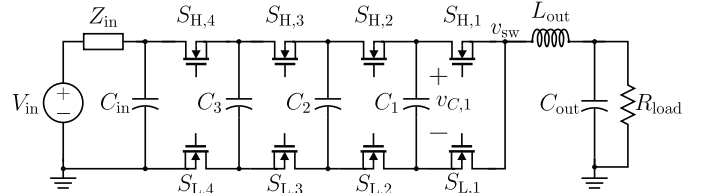


Fig. 1: Simplified five-level FCML converter circuit schematic with input impedance explicitly drawn. The ground-referenced switch-node voltage  $v_{sw}$  is explicitly labeled.

on natural balancing, and derive key equations along with experimental validation.

Several works [10]–[13] have discovered “unbalanced” conversion ratios, at which the flying capacitor voltages theoretically do not passively balance to their desired steady-state values and instead diverge. These “unbalanced” conversion ratios are defined as conversion ratios where  $D \cdot (N - 1)$  and  $(N - 1)$  are not co-prime, where  $D$  is the duty cycle of the high-side switches  $S_{H,k}$  in the FCML converter operated with symmetric phase-shifted PWM (PS-PWM), and where  $D \cdot (N - 1)$  is an integer. Of note, however, is that these theoretically unbalanced operating points and divergent flying capacitor voltages are not typically observed in experimental hardware [11], pointing to a gap in the understanding of all pertinent balancing mechanisms within the converter. Of particular interest in this work is the combination of a five-level FCML converter operated at a duty cycle of  $D = 50\%$  as it is the simplest FCML converter which exhibits this theoretical behavior.

This work analyzes the natural balancing of the capacitor voltages in an FCML converter, and extends past work to also include the impact of switch output capacitance. Crucially, it is discovered that the transient charge flow between flying capacitors and parasitic switch output capacitance  $C_{oss}$  during switch transitions has a naturally balancing effect, which has previously not been documented. A detailed state-space model is developed to include this balancing mechanism, and through hardware validation, it is shown that the proposed model accurately captures the experimental behavior, which was not achieved by previous models.

This work has two key contributions: 1) Identification of the role of the switch output capacitance in the natural balancing of the flying capacitor voltages, along with an analytical expression of the strength of the balancing mechanism. 2)

Development of an analytical model incorporating said balancing mechanism, which shows excellent agreement with experimental results. Together, these two contributions yield — for the first time — a model of FCML converter natural balancing that matches experimental observations during practical operating conditions (e.g., start-up transients). In [14], the authors utilized  $C_{\text{oss}}$ -induced charge flow to actively balance the flying capacitor voltages at zero output current. This manuscript, however, analyzes how  $C_{\text{oss}}$ -induced charge flow participates in the natural balancing process, particularly as it relates to “unbalanced” conversion ratios. Several other works focused on FCML converter design and optimization [15], [16] have considered the power loss penalty of  $C_{\text{oss}}$ , but not this parasitic’s impact on the flying capacitor voltages.

This manuscript is based on our previously published conference publication [17]. In this work, we incorporate the impact of source input impedance and compare its tendency to generate imbalanced flying capacitor voltages to the balancing effect of  $C_{\text{oss}}$ -induced charge flow. Additionally, we include discussion on the incorporation of nonlinear capacitances in an analytical model of the FCML converter. The remainder of this manuscript is organized as follows: Section II introduces the FCML converter and provides a brief overview of natural balancing theory. In Section III, analysis of the charge flow induced by  $C_{\text{oss}}$  and this charge flow’s impact on the flying capacitor voltages is presented. This phenomenon is then incorporated into a state space model for the FCML converter to investigate the transient response of the converter. Section IV shows the experimental setup and data which validate the proposed flying capacitor voltage balancing model. Several FCML converter prototypes are excited with a high slew rate input voltage step and the flying capacitor voltage transient response is analyzed and compared. Finally, Section V concludes this manuscript.

## II. FLYING CAPACITOR MULTILEVEL CONVERTER BALANCING MECHANISMS AND UNBALANCED CONVERSION RATIOS

The promise of the FCML topology to enable the incorporation of high-performance low-voltage switches [16] with an even voltage stress distribution requires that the voltages of the flying capacitors not deviate too far from their ideal distribution. If this constraint is violated, the system efficiency will decrease and in the worst case, the switches will be exposed to a voltage higher than their ratings, yielding converter failure.

Previous works [10], [11], [13], [18]–[21] have analyzed the mechanisms by which the flying capacitors within an FCML converter converge to the balanced steady-state voltage distribution  $v_{C,k} = (kV_{\text{in}})/(N - 1)$  where  $N$  is the number of discrete levels in the switch node waveform, and  $k$  ranges from 1 to  $N - 2$ , with capacitor voltages as annotated in Fig. 1. Work in [9] demonstrated that with symmetric Phase-Shifted PWM (PS-PWM) modulation, the flying capacitor voltages will dynamically balance to the aforementioned voltage distribution. Furthermore, if the high-side switches  $S_{H,k}$  are operated with a duty cycle  $D$ , and the low-side  $S_{L,k}$  switches in a complementary fashion, the output voltage will

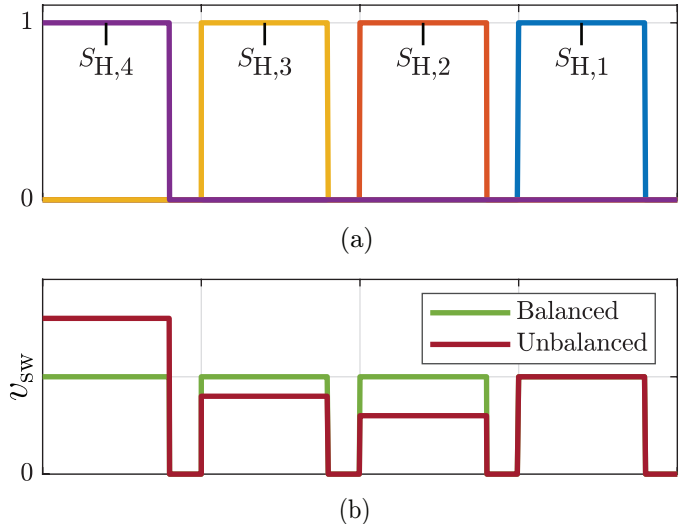


Fig. 2: (a) Example symmetric phase-shifted PWM (PS-PWM) switching signals for a five-level FCML converter operated at a duty cycle  $D = 0.2$ . (b) Switch-node voltage  $v_{\text{sw}}$  resulting from both a balanced and an unbalanced flying capacitor voltage distribution. When the flying capacitor voltages are balanced, the voltage stress applied to the switches and the volt-seconds applied to the output filter inductor are minimized. The unbalanced case shown has flying capacitor voltages of  $v_{C,1} = 0.25V_{\text{in}}$ ,  $v_{C,2} = 0.4V_{\text{in}}$ , and  $v_{C,3} = 0.6V_{\text{in}}$ .

be  $V_{\text{out}} = DV_{\text{in}}$ . Example switching signals and switch node voltages for balanced and unbalanced flying capacitor voltages are shown in Fig. 2.

When the flying capacitor voltages are balanced, the lowest frequencies present in the switch node waveform are dc and  $(N - 1)f_{\text{sw}}$ . According to previous analyses [11], [22], natural balancing occurs because unbalanced flying capacitor voltages create a switch node voltage which has harmonic content between  $f_{\text{sw}}$  and  $(N - 2)f_{\text{sw}}$ , as can be seen in Fig. 2. When these “lower-order” voltage harmonics are present, they induce current and losses in the  $RLC$  circuit of the output filter. These losses work to drive the flying capacitor voltages to their balanced distribution. However, at certain combinations of level count and duty cycle, the flying capacitor voltages are unable to be independently impacted by the  $RLC$  circuit dynamics of the output filter [12], [13] and thus natural balancing fails. Fig. 3 shows the equivalent circuits for a five-level FCML converter operated with symmetric PS-PWM at a duty cycle of 50%. At this operating point, it can be seen that capacitors  $C_1$  and  $C_3$  are always connected in series when connected to the output filter. Since these flying capacitor voltages cannot be independently changed, the flying capacitor voltages theoretically will not balance.

## III. SWITCH OUTPUT CAPACITANCE ( $C_{\text{oss}}$ ) IMPACT ON FLYING CAPACITOR NATURAL BALANCING

To resolve the discrepancy between previous literature and experimental evidence regarding natural balancing at the “unbalanced” conversion ratios [11], [13], there must exist some mechanism not included in the aforementioned works’ simplified model of the FCML converter which acts to drive the flying capacitor voltages to the balanced state, even at

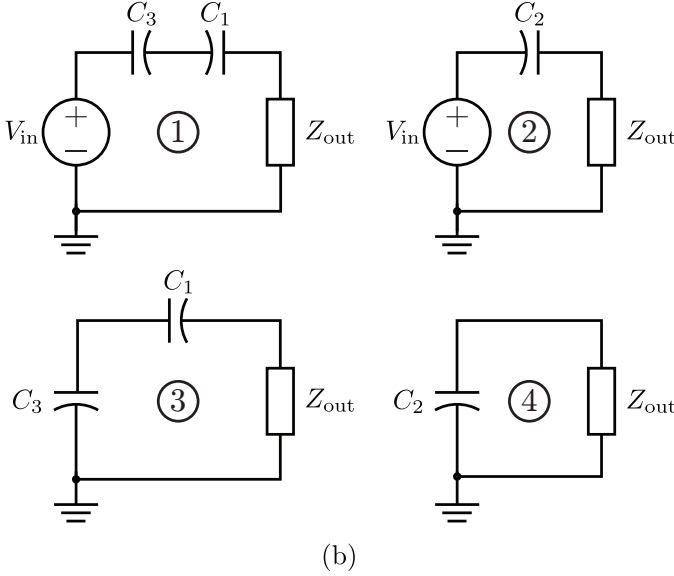
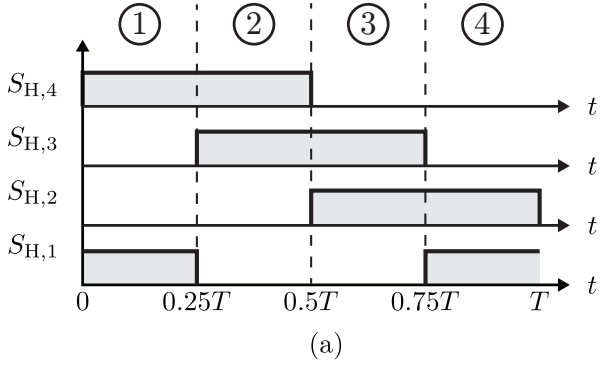


Fig. 3: (a) Gate signals for a five-level FCML converter operated with PS-PWM at a duty cycle of 50%. (b) Equivalent circuits of the FCML converter.  $Z_{out}$  represents the impedance of the output filter inductor and capacitor and load resistance as connected in Fig. 1.

“unbalanced” conversion ratios. One such mechanism not previously modeled is charge redistribution induced by the switch parasitic output capacitance. During each switching event, the output capacitance  $C_{oss}$  of a switch which was previously on is charged from  $\approx 0$  V to a linear combination of the flying capacitor voltages and the input voltage. For example, when  $S_{H,2}$  switches from ON to OFF and  $S_{L,2}$  switches from OFF to ON, the  $C_{oss}$  of  $S_{H,2}$  is charged from  $\approx 0$  V to  $v_{C,2} - v_{C,1}$ . Similarly, the  $C_{oss}$  of  $S_{H,1}$  will be charged from  $\approx 0$  V to  $v_{C,1}$  when  $S_{H,1}$  switches from ON to OFF. As will be shown in the subsequent analysis, these previously unmodeled charge flows due to  $C_{oss}$  are functions of the flying capacitor voltages and provide an inherent balancing mechanism in the FCML converter.

#### A. Charge Flow Analysis

To provide a tractable, analytical description of this charge flow mechanism, we make the following simplifying assumptions: 1) all switches are commuted with zero dead-time and in perfect complementary fashion, and 2) the flying capacitors and  $C_{oss}$  parasitic capacitances are linear. These simplifying assumptions will be examined and re-evaluated in Section III-C. Examining the switching event illustrated in

Fig. 4, at  $t = 0$ ,  $S_{H,2}$  opens and  $S_{L,2}$  closes. The charge quantity circulating during this commutation event can be expressed in terms of the flying capacitor voltages at  $t = 0$  and  $t = t_f$ , where  $t_f$  is the time at which the system voltages have approximately settled. Expressing the charge flowing in the highlighted commutation loop of Fig. 4 as  $Q_{flow}$ :

$$Q_{flow} = C_{oss,H} \Delta v_H = C_{oss,H} \cdot (v_H(t_f) - v_H(0)) \quad (1)$$

$$v_H(t_f) = v_{C,2}(t_f) - v_{C,1}(t_f), \quad v_H(0) \approx 0$$

$$Q_{flow} \approx C_{oss,H} \cdot (v_{C,2}(t_f) - v_{C,1}(t_f)) \quad (2)$$

In this process, charge  $Q_{flow}$  leaves  $C_2$  and is deposited on  $C_1$ . The flying capacitor voltages,  $v_{C,1}$  and  $v_{C,2}$ , after a commutation event are thus functions of this  $Q_{flow}$ :

$$\begin{aligned} v_{C,2}(t_f) &= v_{C,2}(0) - \frac{Q_{flow}}{C_2} \\ &= v_{C,2}(0) - \frac{C_{oss,H}}{C_2} \cdot (v_{C,2}(t_f) - v_{C,1}(t_f)) \\ &= \frac{C_2}{C_2 + C_{oss,H}} v_{C,2}(0) + \frac{C_{oss,H}}{C_2 + C_{oss,H}} v_{C,1}(t_f) \quad (3) \end{aligned}$$

$$\begin{aligned} v_{C,1}(t_f) &= v_{C,1}(0) + \frac{C_{oss,H}}{C_1} \cdot (v_{C,2}(t_f) - v_{C,1}(t_f)) \\ &= \frac{C_1}{C_1 + C_{oss,H}} v_{C,1}(0) + \frac{C_{oss,H}}{C_1 + C_{oss,H}} v_{C,2}(t_f) \quad (4) \end{aligned}$$

Substituting (3) into (4) yields:

$$\begin{aligned} v_{C,1}(t_f) \left[ 1 - \frac{C_{oss,H}^2}{(C_1 + C_{oss,H})(C_2 + C_{oss,H})} \right] &= \\ \frac{C_1}{C_1 + C_{oss,H}} v_{C,1}(0) + \frac{C_{oss,H} C_2}{(C_1 + C_2)(C_2 + C_{oss,H})} v_{C,2}(0). \quad (5) \end{aligned}$$

Finally, by rearranging we obtain an equation for  $v_{C,1}$  at the end of a commutation event:

$$v_{C,1}(t_f) = \frac{v_{C,1}(0) \cdot (C_1 C_2 + C_1 C_{oss,H}) + C_2 C_{oss,H} v_{C,2}(0)}{C_1 C_2 + C_{oss,H} (C_1 + C_2)} \quad (6)$$

As expressed in (6), the flying capacitor voltages rapidly change after a commutation event due to  $C_{oss}$ -induced charge redistribution.

Under the assumption of zero dead-time, both high-to-low switch transitions and low-to-high switch transitions experience the same charge flow. Table I summarizes each flying capacitor voltage after a commutation event (obtained by the same process that yielded (6)). These approximations assume that the commutation events are “local”, that is, only the flying capacitors connected to a commutating switching cell participate in  $C_{oss}$  charge redistribution<sup>1</sup>. Additionally, if two cells commute at the same time, the voltage at the end of the event can be approximated by a cascade of two separate switching events. Note that the entries in Table I are

<sup>1</sup>In reality, flying capacitors that are not directly connected to a switching cell are weakly connected to the cell through the  $C_{oss}$  of a turned OFF switch. For example,  $C_2$  is in parallel with the series combination of  $C_3$  and  $C_{oss}$  when the  $S_2$  switching cell commutes. However, due to the relative sizing of  $C_{fly}$  and  $C_{oss}$  (i.e.,  $C_{fly} \gg C_{oss}$ ) in practical implementations of the topology, the modeling error introduced is negligible.

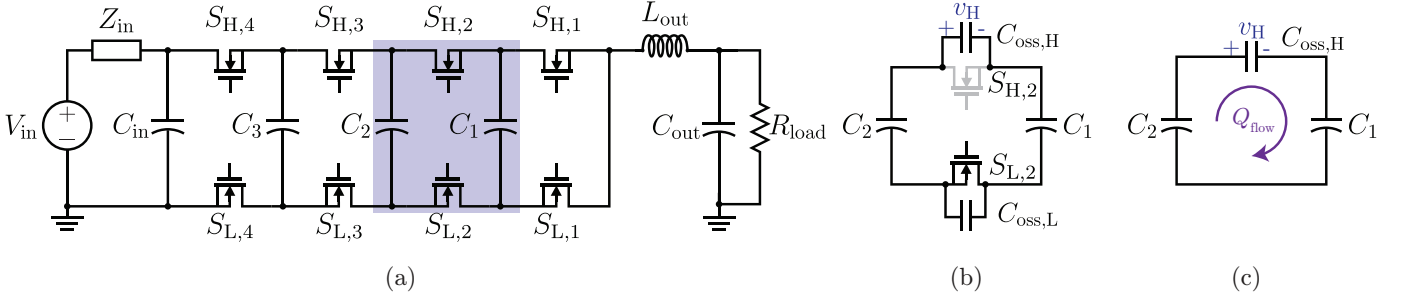


Fig. 4: (a) Simplified five-level FCML converter circuit schematic with source input impedance explicitly drawn and switching cell 2 highlighted. (b) Switching cell 2 with switch output capacitances  $C_{oss}$  explicitly drawn. At  $t = 0$  a commutation of the  $S_2$  switching cell occurs, with  $S_{H,2}$  turning OFF and  $S_{L,2}$  turning ON. (c) Equivalent circuit after  $t = 0$  for analyzing commutation charge flow. Charge  $Q_{flow}$  circulates around the commutation loop, discharging  $C_2$  and charging  $C_1$  and  $C_{oss,H}$ . Parasitic resistances are omitted for clarity.

TABLE I

TABULATED ANALYTICAL SOLUTIONS TO THE FLYING CAPACITOR VOLTAGES AFTER A COMMUTATION EVENT OCCURS FOR  $N=5$ .

Switching Cell Event (ON or OFF)	Flying Capacitor Voltage After Commutation
$S_1$	$v_{C,1}(t_f) = v_{C,1}(0) - \frac{C_{oss}}{C_1 + C_{oss}} v_{C,1}(0)$
$S_2$	$v_{C,1}(t_f) = v_{C,1}(0) + \frac{C_2 C_{oss}}{C_1 C_2 + C_{oss}(C_1 + C_2)} (v_{C,2}(0) - v_{C,1}(0))$ $v_{C,2}(t_f) = v_{C,2}(0) + \frac{C_1 C_{oss}}{C_1 C_2 + C_{oss}(C_1 + C_2)} (v_{C,1}(0) - v_{C,2}(0))$
$S_3$	$v_{C,2}(t_f) = v_{C,2}(0) + \frac{C_3 C_{oss}}{C_2 C_3 + C_{oss}(C_2 + C_3)} (v_{C,3}(0) - v_{C,2}(0))$ $v_{C,3}(t_f) = v_{C,3}(0) + \frac{C_2 C_{oss}}{C_2 C_3 + C_{oss}(C_2 + C_3)} (v_{C,2}(0) - v_{C,3}(0))$
$S_4$	$v_{C,3}(t_f) = v_{C,3}(0) + \frac{C_{oss}}{C_3 + C_{oss}} (V_{in} - v_{C,3}(0))$

generalizable to FCML converters with arbitrary level counts as can be seen by the symmetry in the equations for the  $S_2$  and  $S_3$  switching cell. That is, the form of the equations for switching cell  $S_2$  apply to all switching cells with two flying capacitors.

In reality, commutations are not perfectly instantaneous and practical converters will introduce a deadtime period where  $S_{H,k}$  and  $S_{L,k}$  are OFF simultaneously. These non-zero deadtimes will impact the previously described charge flows in the following ways. For the sake of simplicity, we assume the inductor current  $i_L$  is positive (i.e., flowing to the output in Fig. 4(a)). After  $S_{L,k}$  turns OFF and before  $S_{H,k}$  turns ON, the inductor current  $i_L$  will discharge the  $C_{oss,L}$  of  $S_{L,k}$ . If this capacitance is fully discharged, the body diode (or effective body diode) of this switch will turn ON. If this occurs before  $S_{H,k}$  switch turns on, the low side capacitance will then be charged from  $-V_d$ , the “diode voltage”, up to a combination of the flying capacitor voltages rather than from  $\approx 0$  V as the equations in Table I assume. In practice, this slight approximation error was found to be negligible. Conversely, after  $S_{H,k}$  turns OFF and before  $S_{L,k}$  turns ON,  $C_{oss,H}$  will be partially charged and  $C_{oss,L}$  partially discharged by the inductor current. This will reduce the charge flow when  $S_{L,k}$  turns ON. Similar to neglecting the body diode voltage drop, this approximation error was found to have negligible impact.

### B. Analytical FCML Converter Model Incorporating $C_{oss}$ Induced Charge Flow

Given that the  $C_{oss}$ -induced voltage changes per commutation event are very small compared to the average values of the flying capacitor voltages<sup>2</sup>, it is difficult to ascertain a priori whether the flying capacitor voltages will settle to a balanced state and if they do, how quickly transients settle. To investigate the circuit response, an analytical model was developed in MATLAB to solve for the state variables within the circuit as a function of time. To analytically simulate the circuit, each switching configuration is associated with a set of state-space matrices. As an example, consider the symmetric PS-PWM switch configuration to generate an approximate switch node voltage of  $V_{in}/2$  with switches  $S_{H,1}$ ,  $S_{L,2}$ ,  $S_{L,3}$ , and  $S_{H,4}$  ON while complementary switches are OFF. The circuit associated with this switching configuration is illustrated in Fig. 5. The state-space description of this circuit is:

$$\dot{x}(t) = \frac{d}{dt} \begin{bmatrix} v_{C,1} \\ v_{C,2} \\ v_{C,3} \\ i_L \\ v_{out} \\ v_{C_{in}} \\ i_{Z_{in}} \end{bmatrix} = \mathbf{A} \begin{bmatrix} v_{C,1} \\ v_{C,2} \\ v_{C,3} \\ i_L \\ v_{out} \\ v_{C_{in}} \\ i_{Z_{in}} \end{bmatrix} + \begin{bmatrix} 0 \\ 0 \\ 0 \\ 0 \\ 0 \\ 0 \\ 1 \end{bmatrix} V_{in} \quad (7)$$

<sup>2</sup>For example, in the converter shown in Section III, the flying capacitor voltages may change by less than a tenth of a percent in a commutation event.



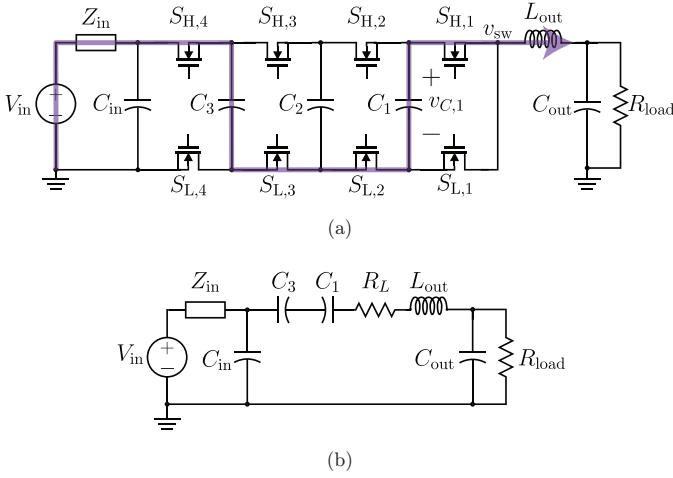


Fig. 5: (a) Circuit schematic of a five-level FCML converter to generate a switch-node voltage of  $V_{in}/2$  with current path highlighted and input network explicitly drawn. (b) Equivalent circuit used to obtain the state space description of Eq. 7.  $R_L$  models the sum of series resistances in the power path (e.g., inductor and FET resistance, etc.).

$$\mathbf{A} = \begin{bmatrix} 0 & 0 & 0 & -C_1^{-1} & 0 & 0 & 0 \\ 0 & 0 & 0 & 0 & 0 & 0 & 0 \\ 0 & 0 & 0 & C_3^{-1} & 0 & 0 & 0 \\ L_{out}^{-1} & 0 & -L_{out}^{-1} & -R_L L_{out}^{-1} & -L_{out}^{-1} & L_{out}^{-1} & 0 \\ 0 & 0 & 0 & C_{out}^{-1} & -C_{out} R_{load}^{-1} & 0 & 0 \\ 0 & 0 & 0 & -C_{in}^{-1} & 0 & 0 & C_{in}^{-1} \\ 0 & 0 & 0 & 0 & 0 & -L_{in}^{-1} & 0 \end{bmatrix} \quad (8)$$

Where  $R_L$  is the sum of series resistances within the sub-circuit comprising inductor resistance, switch on-state resistance, flying capacitor ESR, and any other parasitic resistances.

The state variables at the end of a switching state  $x(t_f)$  are then found by solving the state evolution equation:

$$\dot{x}(t) = \mathbf{A}x(t) + \mathbf{B}V_{in}(t) \quad (9)$$

as a function of the state variables at the beginning of a switching state  $x(t_0)$ . This solution is [23]:

$$x(t_f) = \exp(\mathbf{A}(t_f - t_0))x(t_0) + \int_{t_0}^{t_f} \exp(\mathbf{A}(t_f - \tau))\mathbf{B}V_{in}(\tau)d\tau \quad (10)$$

where  $x(t_0)$  is the initial condition for the state variables and  $x(t_f)$  the final state value. To save memory and computational load, the state variables are only solved at each switching instance, thus the time steps of the solver are the same as those of the switching instances of the converter. By “stitching” together these final and initial states and continually solving the state evolution equation we can obtain time-series data of the converter’s state variables.

To incorporate the charge flows and voltage changes induced by the switch output capacitance, the flying capacitor voltages at the end of a switching state are changed according to Table I. These modified flying capacitor voltages are then used as the initial value for the next state evolution equation solver.

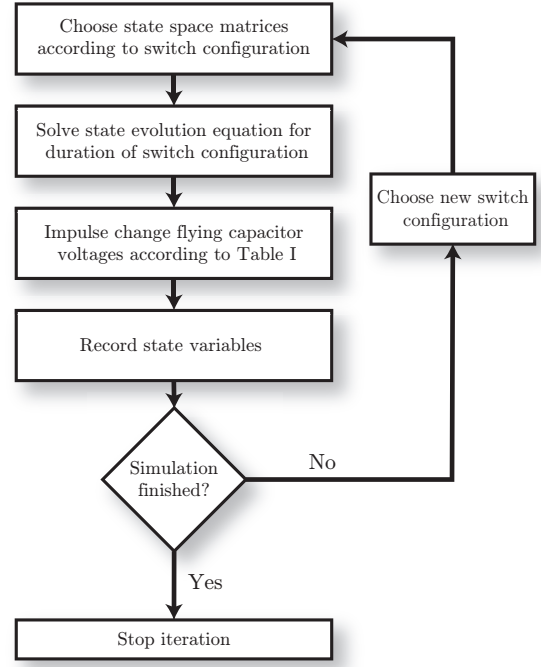


Fig. 6: Flowchart illustrating the MATLAB algorithm developed to obtain the FCML converter state variables as a function of time.

The developed algorithm is shown in the flowchart of Fig. 6.

### C. Extension to Nonlinear Capacitances

In many practical implementations of the FCML topology, nonlinear flying capacitors and nonlinear device  $C_{oss}$  will be employed, requiring an increase in simulation complexity for model fidelity. Class 2 ceramic capacitors (e.g., X6S) are often used for the flying capacitors due to their superior energy density compared to Class 1 capacitors [24]. This benefit in density comes at the penalty of a strongly nonlinear small-signal capacitance versus bias voltage characteristic. To incorporate this impact in an analytical simulation, the state space matrices can be modified by updating the flying capacitance values with a look up table using the flying capacitor voltage at the start of a switching phase. This process implicitly assumes the flying capacitor voltage will not change drastically over a switching phase, an assumption which is generally true in practical implementations.

A more severe nonlinearity is encountered in the transistor output capacitance,  $C_{oss}$ . Fig. 7 depicts the  $C_{oss}$  vs.  $V_{ds}$  curve for the EPC2302 [25], a high performance 100 V eGaN FET. In many implementations, the output capacitance will swing from  $\approx 0$  V to a significant fraction of  $V_{ds,max}$  during a commutation event. Accurate models attempting to capture the impact of  $C_{oss}$  in this operating regime will thus need to include this nonlinearity. At the end of a commutation event, the output capacitance of a switch which was previously ON is charged from  $\approx 0$  V to a combination of the flying capacitor and input voltages. During this process an amount of charge  $Q$  is transferred within the converter. For linear capacitances, this charge is  $Q = CV_{final}$  where  $V_{final}$  is the voltage across

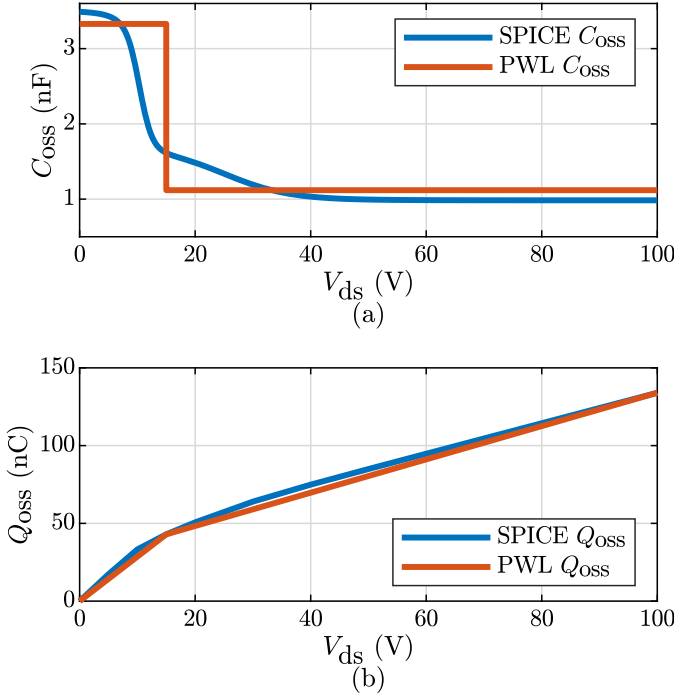


Fig. 7: (a)  $C_{oss}$  characteristics for an example EPC2302 device [25]. Data are obtained by differentiating the manufacturer provided LTSPICE  $Q$ - $v$  curve. (b)  $Q_{oss}$  vs.  $V_{ds}$  for the EPC2302. This curve is well approximated by a two-part piecewise linear (PWL) function.

the  $C_{oss}$  at the end of a commutation event. For nonlinear capacitances however, this charge  $Q$  is a nonlinear function of the final voltage. It is therefore necessary to know the charge flow induced by this voltage change across  $C_{oss}$  to determine the flying capacitor voltages after a commutation event.

Fig. 7(b) shows the  $Q_{oss}$  vs.  $V_{ds}$  curve for the EPC2302 obtained from the manufacturer provided LTSPICE model. Above a certain  $v_{ds}$  voltage (in this case  $\approx 15$  V), the slope of the curve decreases drastically. A faithful approximation is thus obtained through a two-part piecewise linear fit of the curve. This linear fit can be used to approximate the charge flow induced by the charging of the device's  $C_{oss}$  when solving for the flying capacitor voltages after a commutation event. This charge flow is described by

$$Q_{oss}(v) = \begin{cases} C_{high}v & v < V_b \\ C_{high}V_b + C_{low}(v - V_b) & v > V_b \end{cases}. \quad (11)$$

To illustrate this technique, we use the commutation event of the  $S_2$  switching cell in a five-level FCML converter (illustrated in Fig. 4) and assume that  $v_{C,2}(t_f) - v_{C,1}(t_f) > V_b$  as an example.

$$v_{C,2}(t_f) = v_{C,2}(0) - \frac{Q_{flow}}{C_2} \quad (12)$$

$$Q_{flow} = C_{high}V_b + C_{low}(v_{C,2}(t_f) - v_{C,1}(t_f)) \quad (13)$$

Similar to (2), (13) expresses the charge flow as a function of the flying capacitor voltages at the end of a commutation event. The flying capacitor voltages can be solved in a similar manner to that presented in Section III-A.

Fig. 8 shows simulations of a five-level FCML converter

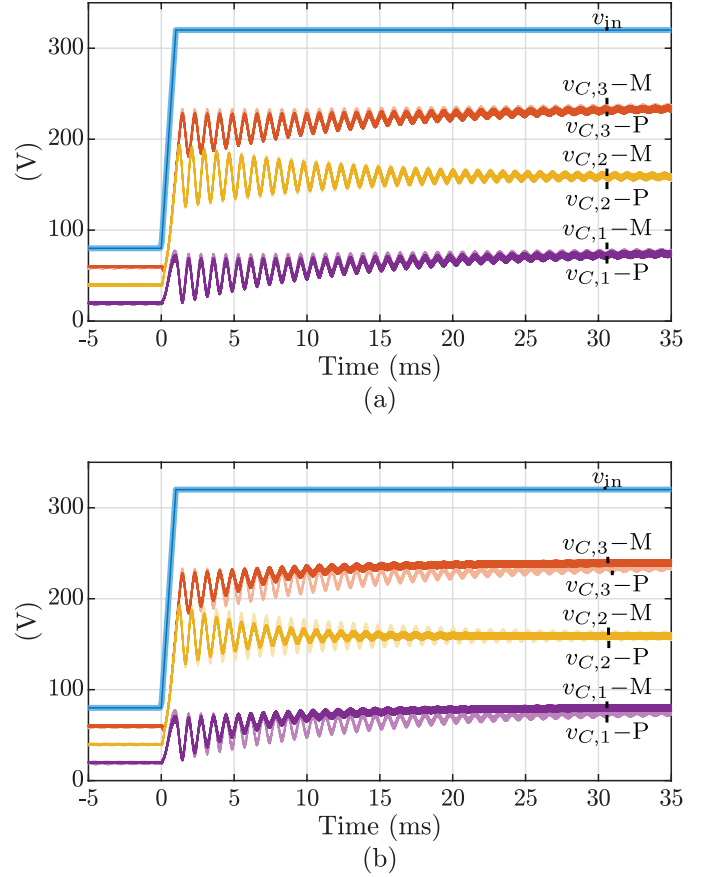


Fig. 8: Transient simulation of a five-level FCML converter including nonlinear  $C_{oss}$ . (a) Analytical model incorporating PWL  $C_{oss}$ . (b) Analytical model assuming a constant  $C_{oss} = C_{oss}(v_{ds} = 0)$ . Traces labeled  $v_{C,i-P}$  are from obtained from PLECS while  $v_{C,i-M}$ , are obtained from an analytical MATLAB simulation. The nonlinear  $C_{oss}$  are implemented in PLECS via variable capacitors and a look up table derived from the EPC2302 [25] datasheet.

which demonstrates the inclusion of the nonlinear  $C_{oss}$  and a piecewise linear approximation as a comparison. This simulation operates at a significantly higher  $v_{in}$ , up to 320 V. At this input voltage, the  $v_{ds}$  of the switches is up to 80 V, a large enough voltage to encounter the nonlinearity in the  $C_{oss}(v_{ds})$  curve. A PLECS simulation using variable capacitors and look up tables implements the nonlinear  $C_{oss}$  curve from the EPC2302 [25] datasheet. Fig. 8(a) implements the piecewise linear  $C_{oss}$  model described above while Fig. 8(b) assumes that the  $C_{oss}$  is constant at the value of  $C_{oss}(v_{ds} = 0)$ . Since  $C_{oss}(v_{ds})$  drops significantly above  $v_{ds} = V_b$ , assuming a constant  $C_{oss}$  predicts a circuit that exhibits a more damped response than the PLECS simulation.

#### D. Comparison to Insufficient Input Capacitance

The balancing mechanism produced by  $C_{oss}$ -induced charge flow serves to work in tandem with natural balancing and combat other imbalance mechanisms. One such imbalance mechanism found to have a significant impact in [18], [26] is that of input voltage ripple due to insufficient input capacitance. The authors in [18], [26] found that this imbalance mechanism had a much stronger impact than other mechanisms (e.g., gate driver delay mismatch).



TABLE II  
SIMULATION PARAMETERS FOR STUDY IN SECTION III-D

Parameter	Value	Parameter	Value
$V_{in}$	50 V	$R_{load}$	$2 \Omega$
$L_{in}$	$1 \mu\text{H}$	$C_{out}$	$44 \mu\text{F}$
$R_{in}$	$0.1 \Omega$	$L_{out}$	$10 \mu\text{H}$
$f_{sw}$	120 kHz	$D$	0.251
$C_{fly}$	$5 \mu\text{F}$	$C_{oss}$	$3.5 \text{ nF}$

TABLE III  
CIRCUIT PARAMETERS USED IN EXPERIMENT IN FIG. 12

Component	Description	Part Name
Power Semicond.	200 V, 10 m $\Omega$ , 450 pF*	EPC2034
$C_{fly}$	$4.4 \mu\text{F}$	C5750X6S2W225K250KA
$L_{out}$	$7.5 \mu\text{H}$	XAL1510-153
$C_{out}$	$0.6 \mu\text{F}$	C5750C0G2J104J280KC

\*This is the  $C_{oss}$  for  $v_{ds} = V_{rated}/2$ .

To compare the impacts of the  $C_{oss}$ -induced balancing mechanism and the insufficient input capacitance unbalancing mechanism, a simulation study was performed. In one simulation the influence of  $C_{oss}$ -induced charge flow is included while in the other, a traditional simulation (i.e., one without  $C_{oss}$ ) is performed. The results of this study for a five-level FCML converter are shown in Fig. 9 with simulation parameters reported in Table II. A model excluding  $C_{oss}$  significantly overpredicts the steady-state error of the flying capacitor voltages. Although a model including  $C_{oss}$  accurately predicts a slight steady-state error,  $C_{oss}$ -induced charge flows drive the converter closer to the ideal balanced voltage distribution. Thus, including the impact of the  $C_{oss}$  charge flows in a converter model will predict a more realistic flying capacitor voltage distribution. Note, the steady-state values reported are the midrange of the capacitor voltage waveform (i.e.,  $[\max(v_{C,k}) - \min(v_{C,k})]/2$ ).

This example illustrates a key aspect of  $C_{oss}$ -induced balancing: The  $C_{oss}$ -induced charge flows by no means guarantee that the flying capacitor voltages will be perfectly balanced. Known imbalance mechanisms such as gate driver delay mismatch, switch on-resistance mismatch, and insufficient input capacitance work in opposition to  $C_{oss}$  charge flows and may result in a flying capacitor voltage distribution that deviates from the ideal. Additionally, the “strength” of the  $C_{oss}$ -induced balancing mechanism depends on both  $C_{oss}$  and the capacitance of the flying capacitors  $C_{fly}$ . Larger  $C_{oss}$  and smaller  $C_{fly}$  result in a more pronounced  $C_{oss}$ -induced balancing impact.

#### IV. EXPERIMENTAL VALIDATION

To validate the theory of  $C_{oss}$ -induced natural balancing of the flying capacitor voltages, we imposed input voltage transients on several five-level FCML converter hardware prototypes and observed the oscillatory response of the flying capacitor voltages and the time-domain response of the circuit. To experimentally observe all pertinent frequencies, the step input voltage excitation must have a rise time sufficiently

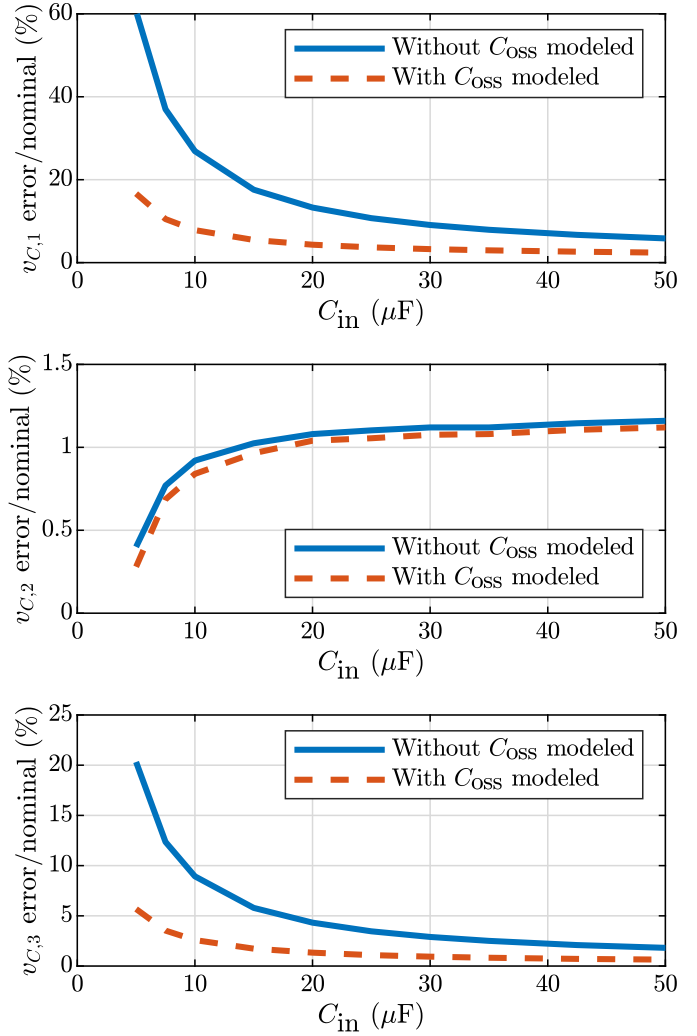


Fig. 9: Simulation study results investigating the steady-state error distribution of flying capacitor voltages. Including the impact of  $C_{oss}$ -induced charge flow predicts a more balanced distribution of flying capacitor voltages than a model without. Reported voltages are the midrange of the flying capacitor voltage waveform.

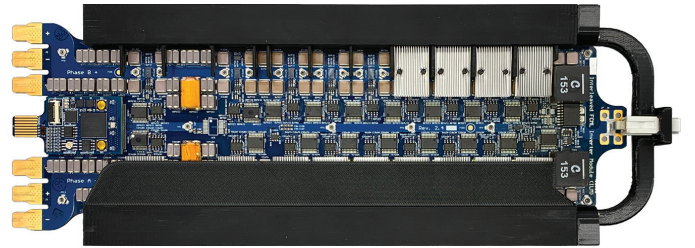


Fig. 10: A top-down view of the ten-level FCML converter prototype [5] used to obtain the experimental data shown in Fig. 12. Each PCB contains two, interleaved ten-level FCML converters switching at a frequency of 115 kHz with  $LC$  filters on board. Circuit parameters are given in Table III. The converter is configured for five-level operation by turning ON switches  $S_{H,5-9}$  and  $S_{L,5-9}$ . One of the two FCML converters is left disconnected for the experiments performed in this work.

fast to excite higher frequency oscillations. To accomplish this, the circuit highlighted in the top left of Fig. 11 was devised. Before the step occurs, the gate of the MOSFET  $S_{tr}$  is held low (where  $S(t)$  is the switching signal applied to  $S_{tr}$ ) and  $V_{in,FCML} = V_{in} - V_Z$ , where  $V_Z$  is the Zener

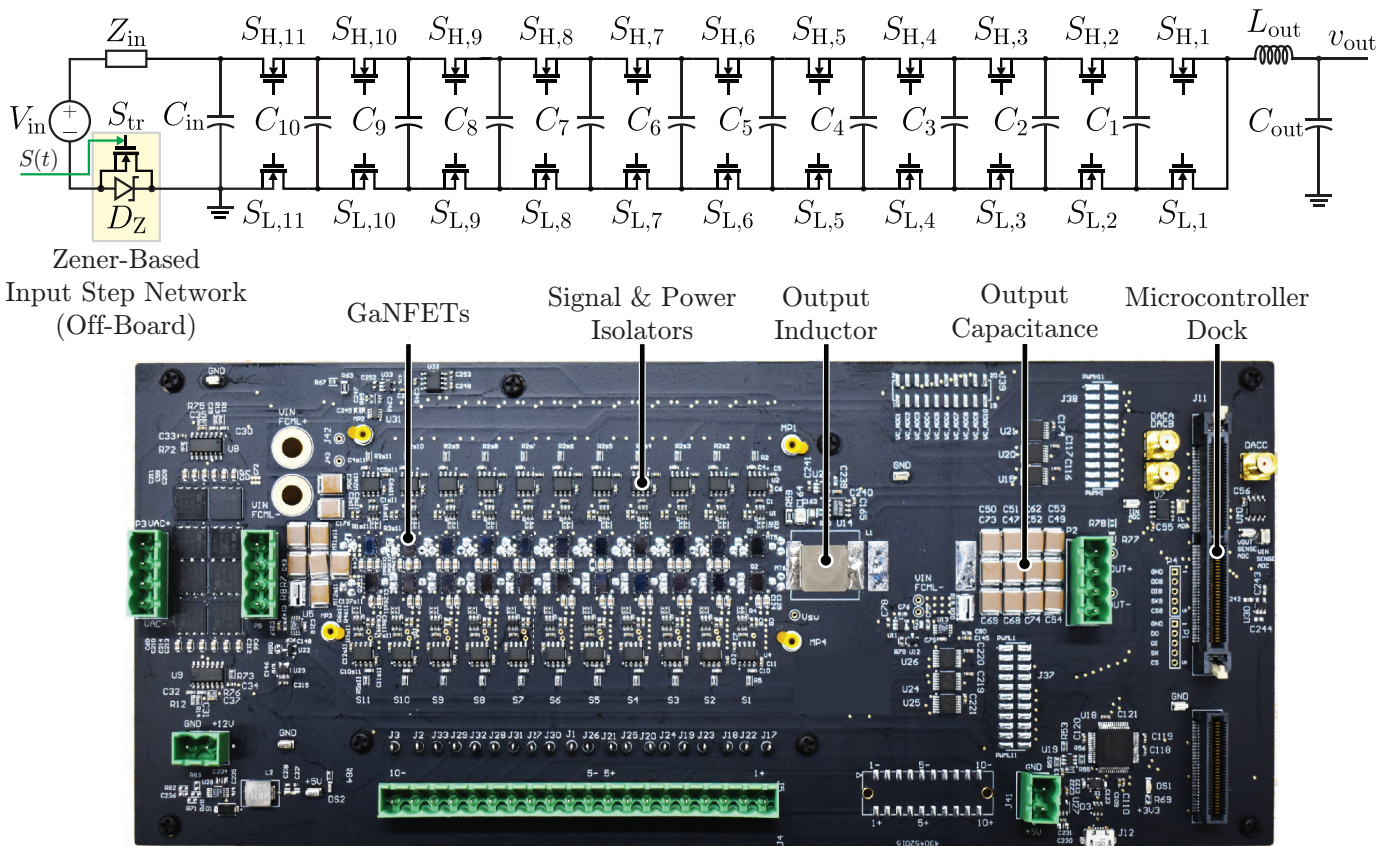


Fig. 11: Hardware photograph of prototype 2, a twelve-level FCML converter configured for five-level operation for the experiments performed in Fig. 13. Highlighted in the top left corner of the figure is the input step network. By adjusting the switching signal  $S(t)$  from OFF to ON, the input voltage to the FCML is raised from  $V_{in} - V_Z$  to  $V_{in}$  where  $V_Z$  is the Zener voltage of the external Zener diode  $D_Z$  in series with the input port of the FCML converter. The converter is configured for five-level operation by turning ON switches  $S_{H,5-11}$  and  $S_{L,5-11}$ . Pertinent component parameters are given in Table IV.

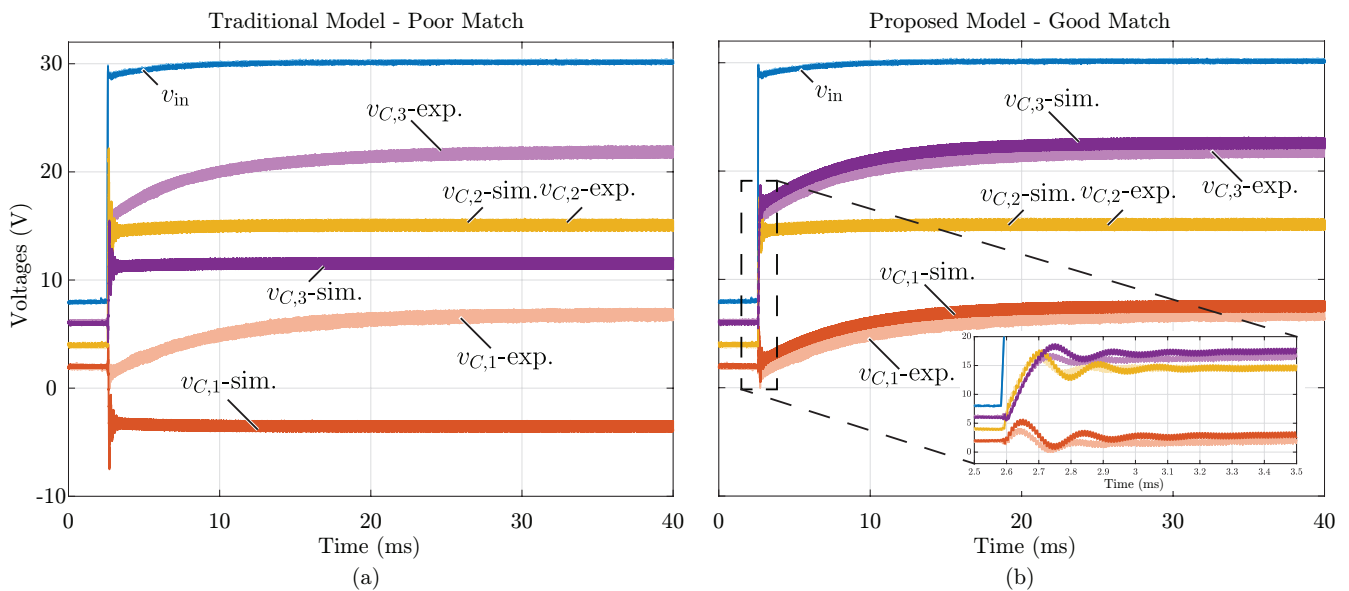


Fig. 12: Measured data from prototype 1, a five-level FCML [5] shown in Fig. 10. The FCML converter was excited with an  $\approx 22.5$  V input voltage step by the input step network highlighted in the top left of Fig. 11 while operating at a duty cycle of 50%. Waveforms labeled “-sim.” are simulation data while those labeled “-exp.” are experimental data. (a) A simulation of a traditional model (i.e., one that does not include the impact of  $C_{OSS}$ ) compared with experiment. This model is clearly deficient in modeling the flying capacitor voltages’ transient response. (b) Transient response of model including the impact of  $C_{OSS}$  which predicts the flying capacitors natural convergence to their balanced values as experiment does. The inset in (b) shows a zoomed in view of the initial transient response of the flying capacitor voltages, which exhibits an oscillatory behavior. Both simulations employed the algorithm shown in Fig. 6.

TABLE IV  
CIRCUIT PARAMETERS USED IN EXPERIMENTS IN FIG. 13

Component	Description	Part Name
Power Semicond.	100 V, 1.8 m $\Omega$ , 1 nF*	EPC2302
$C_{\text{fly}}$	8.8 $\mu\text{F}$	C5750X6S2W225K250KA
$L_{\text{out}}$	10 $\mu\text{H}$	IHL P5050CEER100M01
$C_{\text{out}}$	44 $\mu\text{F}$	C5750C0G2J104J280KC

\*This is the  $C_{\text{oss}}$  for  $v_{\text{ds}} = V_{\text{rated}}/2$ .

TABLE V  
PROTOTYPE PARAMETER COMPARISON

Parameter	Ratio
$R_{\text{ds},1}/R_{\text{ds},2}$	5.5
$C_{\text{fly},1}/C_{\text{fly},2}$	2
$C_{\text{out},1}/C_{\text{out},2}$	73
$C_{\text{oss},1}/C_{\text{oss},2}$	0.5

voltage, is applied to the FCML converter’s input port. To activate the step, the gate of  $S_{\text{tr}}$  is pulled high, increasing the input voltage to the converter to  $V_{\text{in}}$  at a high slew rate. The outputs of both converters were connected to a constant 9.8  $\Omega$  load. To add further experimental evidence of the proposed  $C_{\text{oss}}$ -induced balancing theory, two FCML converter prototypes were developed. The prototypes differ significantly in converter parameters found to influence natural balancing dynamics. A summary of the differences in the two prototypes is provided in Table V.

#### A. Prototype 1 Validation

Presented in Fig. 12 are the results from this input voltage step study applied to the FCML converter shown in Fig. 10. As can be seen, both the analytical simulation and measured results agree very well when including the impact of  $C_{\text{oss}}$ -induced charge flow on the FCML converter as derived in Section III. If the impact of  $C_{\text{oss}}$  is not included and the FCML converter is modeled in the traditional way, the flying capacitor voltages will not converge to a balanced state as experiment does. These results are significant as they indicate that previous models of the FCML converter were inadequate as they neglected a key parasitic element in the circuit rather than a flaw in the analysis of the simplified circuit. The converter was operated with symmetric PS-PWM at a constant switching frequency of 115 kHz.

#### B. Prototype 2 Validation

Fig. 13(a) shows the transient response of prototype 2, shown in Fig. 13(b), while operating at a “balanced” conversion ratio of 25%. Since the  $RLC$  circuit dynamics investigated in previous works [22], [27] are now able to participate in driving the flying capacitors to their balanced voltages at this conversion ratio, the flying capacitor voltages converge much faster to their balanced values compared to the case of a conversion ratio of 50%, shown in Fig 13(b). The component parameters are given in Table IV and the converter was operated at a switching frequency of 75 kHz. The six highest

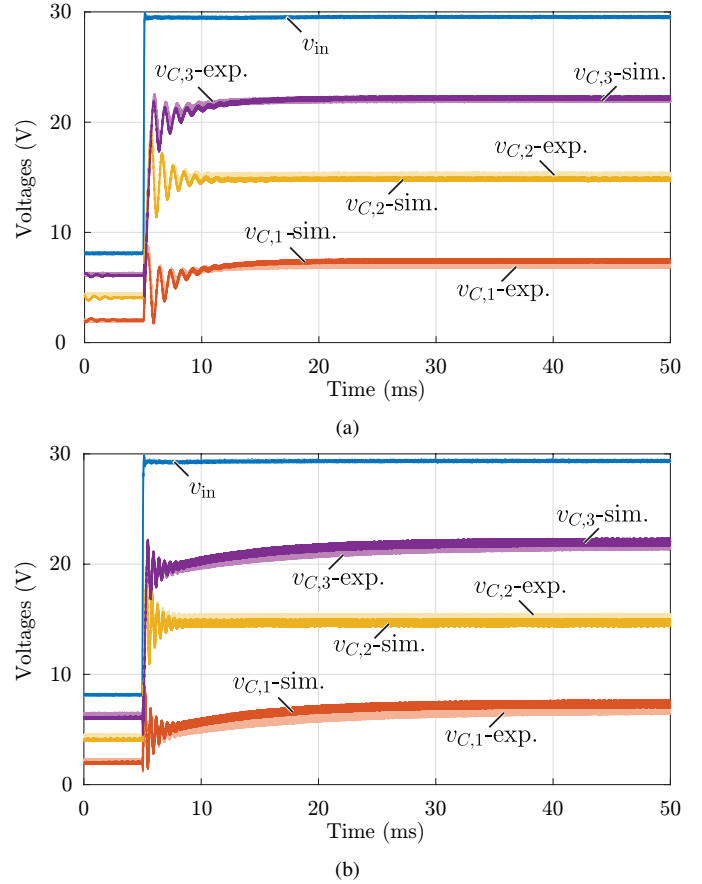


Fig. 13: Measured data from prototype 2, a five-level FCML shown in Fig. 11. (a) operated at a “balanced” conversion ratio of 25% and (b) an “unbalanced” conversion rate 50%. The input port of the FCML converter was excited with the same input voltage excitation as the experiment presented in Fig. 12. Compared to the experiment presented in Fig. 12, prototype 2 operates at a slower switching frequency (65%) and utilizes a larger output capacitor (73 $\times$ ). Despite these differences the presented model and experiment agree quite well. Waveforms labeled “-sim.” are simulation data while those labeled “-exp.” are experimental data.

voltage switch pairs were held constantly ON to generate the five-level converter.

## V. CONCLUSION

This work has analyzed a key parasitic element, the switch output capacitance  $C_{\text{oss}}$ , and its impact on the ability of the flying capacitors within a FCML converter to balance to their desired voltages. Without the inclusion of this previously neglected balancing mechanism, simulation and analytical models of the FCML converter are unable to track experimental data. Ensuring model fidelity of the FCML converter is critical for both flying capacitor voltage estimation (e.g., for converter health monitoring) and active balancing control of the flying capacitor voltages. Although  $C_{\text{oss}}$ -induced balancing reduces switch voltage stress and inductor current harmonics, the flying capacitor voltages are balanced through a lossy mechanism. That is, FCML implementations which do not exhibit soft-switching will incur increased switching and/or overlap losses due to increased  $C_{\text{oss}}$ . Thus, attempts to force balanced flying capacitor voltages through increased  $C_{\text{oss}}$  will be met with increased switching losses. Using the modeling



techniques presented in this paper, the designer can assess the impact of parasitic device  $C_{oss}$  and whether additional external capacitance is beneficial.

#### ACKNOWLEDGMENTS

The authors would like to thank the Fannie and John Hertz Foundation for supporting this work.

#### REFERENCES

- [1] R. Jansen, G. V. Brown, J. L. Felder, and K. P. Duffy, "Turboelectric Aircraft Drive Key Performance Parameters and Functional Requirements," in *51st AIAA/SAE/ASEE Joint Propulsion Conference*. Orlando, FL: American Institute of Aeronautics and Astronautics, Jul. 2015. [Online]. Available: <http://arc.aiaa.org/doi/10.2514/6.2015-3890>
- [2] E. Masanet, A. Shehabi, N. Lei, S. Smith, and J. Koomey, "Recalibrating global data center energy-use estimates," *Science*, vol. 367, no. 6481, pp. 984–986, Feb. 2020. [Online]. Available: <https://www.science.org/doi/10.1126/science.aba3758>
- [3] ABB, "Energy efficiency - Motors and Drives Infographic," Dec. 2018. [Online]. Available: <https://library.abb.com/d/3AUA0000182864>
- [4] Y. Lei, C. Barth, S. Qin, W.-C. Liu, I. Moon, A. Stillwell, D. Chou, T. Foulkes, Z. Ye, Z. Liao, and R. C. N. Pilawa-Podgurski, "A 2-kW Single-Phase Seven-Level Flying Capacitor Multilevel Inverter With an Active Energy Buffer," *IEEE Transactions on Power Electronics*, vol. 32, no. 11, pp. 8570–8581, Nov. 2017.
- [5] N. Pallo, S. Coday, J. Schaadt, P. Assem, and R. C. N. Pilawa-Podgurski, "A 10-Level Flying Capacitor Multi-Level Dual-Interleaved Power Module for Scalable and Power-Dense Electric Drives," in *2020 IEEE Applied Power Electronics Conference and Exposition (APEC)*, Mar. 2020, pp. 893–898.
- [6] Z. Liao, D. Chou, K. Fernandez, Y.-L. Syu, and R. C. N. Pilawa-Podgurski, "Architecture and Control of An Interleaved 6-Level Bidirectional Converter With an Active Energy Buffer for Level-II Electric Vehicle Charging," in *2020 IEEE Energy Conversion Congress and Exposition (ECCE)*. Detroit, MI, USA: IEEE, Oct. 2020, pp. 4137–4142.
- [7] J. Azurza Anderson, E. J. Hanak, L. Schrittwieser, M. Guacci, J. W. Kolar, and G. Deboy, "All-Silicon 99.35% Efficient Three-Phase Seven-Level Hybrid Neutral Point Clamped/Flying Capacitor Inverter," *CPSS Transactions on Power Electronics and Applications*, vol. 4, no. 1, pp. 50–61, Mar. 2019.
- [8] S. Coday, N. Ellis, N. Stokowski, and R. C. N. Pilawa-Podgurski, "Design and Implementation of a (Flying) Flying Capacitor Multilevel Converter," in *2022 IEEE Applied Power Electronics Conference and Exposition (APEC)*, Mar. 2022, pp. 542–547.
- [9] T. A. Meynard and H. Foch, "Multi-level conversion: high voltage choppers and voltage-source inverters," in *PESC '92 Record. 23rd Annual IEEE Power Electronics Specialists Conference*, Jun. 1992, pp. 397–403 vol.1.
- [10] S. Thielemans, A. Ruderman, B. Reznikov, and J. Melkebeek, "Improved Natural Balancing With Modified Phase-Shifted PWM for Single-Leg Five-Level Flying-Capacitor Converters," *IEEE Transactions on Power Electronics*, vol. 27, no. 4, pp. 1658–1667, Apr. 2012.
- [11] R. H. Wilkinson, "Natural Balancing of Multicell Converters," Ph.D. dissertation, University of Stellenbosch, 2004.
- [12] R. H. Wilkinson, T. A. Meynard, and H. du Toit Mouton, "Natural Balance of Multicell Converters: The General Case," *IEEE Transactions on Power Electronics*, vol. 21, no. 6, pp. 1658–1666, Nov. 2006.
- [13] Z. Xia, B. L. Dobbins, and J. T. Stauth, "Natural Balancing of Flying Capacitor Multilevel Converters at Nominal Conversion Ratios," in *2019 20th Workshop on Control and Modeling for Power Electronics (COMPEL)*, Jun. 2019, pp. 1–8.
- [14] P. Czyz, P. Papamanolis, F. Trunas Bruguera, T. Guillod, F. Krismer, V. Lazarevic, J. Huber, and J. W. Kolar, "Load-Independent Voltage Balancing of Multi-Level Flying Capacitor Converters in Quasi-2-Level Operation," *Electronics*, vol. 10, no. 19, p. 2414, Oct. 2021.
- [15] N. Pallo, "High-Performance Architectures for Vehicle Propulsion: An Unconventional Approach to Design, Fabrication and Analysis using Scalable Flying Capacitor Multilevel Converter Modules," PhD Thesis, EECS Department, University of California, Berkeley, Aug. 2021.
- [16] J. Azurza Anderson, G. Zulauf, J. W. Kolar, and G. Deboy, "New Figure-of-Merit Combining Semiconductor and Multi-Level Converter Properties," *IEEE Open Journal of Power Electronics*, vol. 1, pp. 322–338, 2020.

- [17] R. S. Bayliss, N. C. Brooks, and R. C. N. Pilawa-Podgurski, "On the Role of Switch Output Capacitance on Passive Balancing within the Flying Capacitor Multilevel Converter," in *2022 IEEE 23rd Workshop on Control and Modeling for Power Electronics (COMPEL)*, Jun. 2022, pp. 1–6.
- [18] Z. Ye, Y. Lei, Z. Liao, and R. C. N. Pilawa-Podgurski, "Investigation of Capacitor Voltage Balancing in Practical Implementations of Flying Capacitor Multilevel Converters," *IEEE Transactions on Power Electronics*, vol. 37, no. 3, pp. 2921–2935, Mar. 2022.
- [19] A. Ruderman, B. Reznikov, and M. Margaliot, "Simple analysis of a flying capacitor converter voltage balance dynamics for DC modulation," in *2008 13th International Power Electronics and Motion Control Conference*. Poznan, Poland: IEEE, Sep. 2008, pp. 260–267.
- [20] A. Ruderman and B. Reznikov, "Five-level single-leg flying capacitor converter voltage balance dynamics analysis," in *2009 35th Annual Conference of IEEE Industrial Electronics*. Porto, Portugal: IEEE, Nov. 2009, pp. 486–491.
- [21] Xiaoming Yang, H. Stemmler, and I. Barbi, "Self-balancing of the clamping-capacitor-voltages in the multilevel capacitor-clamping-inverter under sub-harmonic PWM modulation," *IEEE Transactions on Power Electronics*, vol. 16, no. 2, pp. 256–263, Mar. 2001.
- [22] T. Meynard, M. Fadel, and N. Aouda, "Modeling of multilevel converters," *IEEE Transactions on Industrial Electronics*, vol. 44, no. 3, pp. 356–364, Jun. 1997.
- [23] M. Dahleh, M. Dahleh, and G. Verghese, *Lectures on Dynamic Systems and Control*. Massachusetts Institute of Technology: MIT OpenCourseWare, <https://ocw.mit.edu/>, 2011.
- [24] J. Zou, N. C. Brooks, S. Coday, N. M. Ellis, and R. C. N. Pilawa-Podgurski, "On the Size and Weight of Passive Components: Scaling Trends for High-Density Power Converter Designs," in *2022 IEEE 23rd Workshop on Control and Modeling for Power Electronics (COMPEL)*, Jun. 2022, pp. 1–7.
- [25] EPC Corporation, "EPC2302 Datasheet," Mar. 2023.
- [26] Z. Ye, Y. Lei, Z. Liao, and R. C. N. Pilawa-Podgurski, "Investigation of capacitor voltage balancing in practical implementations of flying capacitor multilevel converters," in *2017 IEEE 18th Workshop on Control and Modeling for Power Electronics (COMPEL)*, Jul. 2017, pp. 1–7.
- [27] B. P. McGrath and D. G. Holmes, "Analytical Modelling of Voltage Balance Dynamics for a Flying Capacitor Multilevel Converter," *IEEE Transactions on Power Electronics*, vol. 23, no. 2, pp. 543–550, Mar. 2008.



**Roderick S. Bayliss III** (Student Member, IEEE) received his B.S. and M.Eng. degrees in electrical engineering from the Massachusetts Institute of Technology, Cambridge, MA, USA, in 2020 and 2021. He is currently working toward the Ph.D. degree in Electrical Engineering with the Department of Electrical Engineering and Computer Sciences, University of California, Berkeley, Berkeley, CA, USA.

After internships at Tesla, Inc. and SpaceX, he joined the Pilawa Group at UC Berkeley. His research interests include multilevel power converter design and control and high performance power magnetics design.

Mr. Bayliss III was a recipient of the UC Berkeley Chancellor's Fellowship and the Hertz Fellowship.



**Nathan C. Brooks** (Member, IEEE) received the B.S. degree from the Rose-Hulman Institute of Technology, Terre Haute, IN, USA, in 2016, and the M.S. degree from the University of Illinois at Urbana-Champaign, Champaign, IL, USA, in 2018, both in electrical engineering, and the Ph.D. degree in electrical engineering and computer sciences from the University of California at Berkeley, Berkeley, CA, USA, in 2023.

He is currently an Assistant Professor with Electrical and Computer Engineering Department, Rose-Hulman Institute of Technology. His research interests include dynamic modeling of switched circuits, high-performance circuit layout, passive component characterization, and high-density design of single-phase and multilevel power converters. His teaching interests include introductory circuit analysis, introductory control systems, signal processing, and power electronics.



**Robert C. N. Pilawa-Podgurski** (Fellow, IEEE) (S'06–M'11–SM'19–F'24) was born in Hedemora, Sweden. He is currently a Professor in the Electrical Engineering and Computer Sciences Department at the University of California, Berkeley, and is the founding director of the Berkeley Power and Energy Center (BPEC). Previously, he was an Associate Professor in Electrical and Computer Engineering at the University of Illinois Urbana-Champaign. He received dual B.S. degrees in physics and electrical engineering and computer science in 2005, the

M.Eng. degree in electrical engineering and computer science in 2007, and the Ph.D. degree in electrical engineering in 2012, all from the Massachusetts Institute of Technology. He performs research in the area of power electronics, and enjoys coaching soccer. His research interests include renewable energy applications, electric vehicles, CMOS power management, high density and high efficiency power converters, data center power delivery, and advanced control of power converters.

Dr. Pilawa-Podgurski served as the Student Activities Chair for IEEE Energy Conversion Congress and Exposition 2016 & 2017, and as the Technical Co-Chair for the 4th IEEE Workshop on Wide Bandgap Power Devices and Applications, 2016. From 2014 to 2022, he served the PELS Technical Committee 6 – Emerging Power Electronics Technologies as Awards Chair, Secretary, Vice Chair, and Chair. From 2016-2019 he served as Chair of PELS Technical Committee 2—Power Conversion Systems and Components. From 2014-2019, he served as Associate Editor for IEEE Transactions on Power Electronics, and for IEEE Journal of Emerging and Selected Topics in Power Electronics. From 2018-2023, he was a member of the IEEE ISSCC Power Management Committee.

Dr. Pilawa-Podgurski received the Chorafas Award for outstanding MIT EECS Master's thesis, the Google Faculty Research Award in 2013, and the 2014 Richard M. Bass Outstanding Young Power Electronics Engineer Award of the IEEE Power Electronics Society, given annually to one individual for outstanding contributions to the field of power electronics before the age of 35. In 2015, he received the Air Force Office of Scientific Research Young Investigator Award, the UIUC Dean's Award for Excellence in Research in 2016, the UIUC Campus Distinguished Promotion Award in 2017, and the UIUC ECE Ronald W. Pratt Faculty Outstanding Teaching Award in 2017. He was the 2018 recipient of the IEEE Education Society Mac E. Van Valkenburg Award given for outstanding contributions to teaching unusually early in his career. In 2023, he received the UC Berkeley EECS department Electrical Engineering Outstanding Teaching Award. He is co-author of seventeen IEEE prize papers.